CSMA 2022
15ème Colloque National en Calcul des Structures
16-20 Mai 2022, Presqu'île de Giens (Var)

Model order reduction of nonlinear MEMS structures: a high order invariant manifold approach

A. Opreni[1], A. Vizzaccaro[2], G. Gobat[1], A. Martin[3],
L. Salles[4], A. Frangi[1], C. Touzé[3]

[1] *Department of Civil and Environmental Engineering, Politecnico di Milano, {andrea.opreni,giorgio.gobat,attilio.frangi}@polimi.it*
[2] *Department of Engineering Mathematics, University of Bristol, alessandra.vizzaccaro@bristol.ac.uk*
[3] *ENSTA Paris-CNRS-EDF-CEA-Institut Polytechnique de Paris, {adrien.martin,cyril.touze}@ensta-paris.fr*
[4] *Skolkovo Institute of Science and Technology, l.salles@skoltech.ru*

Résumé — A high order direct parametrisation of invariant manifolds is exploited to operate dimensionality reduction for vibrating structures subjected to geometric nonlinearities. The method defines a nonlinear coordinate change between the nodal degrees-of-freedom and the normal coordinates, hence expressing the dynamics in an invariant-based span of the phase space. The method is applied to study micro-electro-mechanical systems (MEMS) subjected to geometric nonlinearities and internal resonance. Remarks on the computational performance are reported to highlight the efficiency of the technique.
Mots clés — model order reduction, invariant manifold theory, MEMS

1 Introduction

Nonlinear vibrations of structures featuring internal resonance represent a key research area in the semiconductor industry [1]. In particular, the problem of computing the nonlinear dynamic response of MEMS structures operating at large amplitudes represent today the main challenge associated to the design of this class of system since nonlinear terms break invariance of the linear trial subspace, hence making linear projection techniques as the modal projection or the proper orthogonal decomposition difficult to apply in an efficient and automated manner [2, 3]. As a consequence, starting from the seminal work of Shaw and Pierre on the concept of Nonlinear Normal Mode (NNM) [4], research on dimensionality reduction techniques for geometrically nonlinear structures transitioned from linear to nonlinear methods, i.e. techniques aimed at parametrising the system motion along the invariant manifolds that are the continuations of the linear eigenspaces. The available literature on the topic is vast and a recent review on the topic has been recently published [5]. Within the framework of dimensionality reduction of Finite Element (FE) systems, methods that use a nonlinear mapping to improve model order reduction techniques have already been applied, as for instance the Quadratic Manifold (QM) [6] and the Implicit Condensation (IC) [7, 8]. However, as shown for example in [9, 10, 11], these methods neglect the velocity dependance in the nonlinear coordinate change, and thus are prone to fail as soon as a clear slow-fast separation between master and slave coordinates is not at hand. On the other hand, a complete different approach is that provided by methods that account for the velocity dependence of the manifold. This class of methods leverage the parametrisation method for invariant manifolds formulated by Cabré, Fontich and de la Llave [12, 13, 14] to parametrise the system motion along the manifold of interest. Theory and algorithmic aspects of the method are detailed in the book by Haro [15]. While the normal form has already been applied for model order reduction in early works as in [16], the parametrisation method with a normal form style has been automated for the first time in [17], thus offering solutions with arbitrary orders of expansions. The main limitation of this class of methods is the necessity to operate in modal representation, which is unfeasible for large finite element systems. Recent developments on the topic overcame this issue by introducing a change of coordinates between physical and master coordinates, hence avoiding the computation of the full eigenspectrum of the system [18, 19, 20]. In the present work we exploit the direct parametrisation procedure detailed in [21] for the analysis of MEMS structures of industrial relevance.
The remainder of the paper is organised as follows. In Section 2 a brief overview of the Direct Parame-

trisation for Invariant Manifolds (DPIM) in vibratory systems is reported. In Section 3 the benefits of a high order parametrisation are highlighted on a MEMS micromirror developed by STMicroelectronics®. In Section 4 a high order graph style parametrisation is applied to derive a reduced model of an arch resonator that features a 1 :2 internal resonance. Finally, in Section 5 final remarks and future prospective for the presented method are detailed.

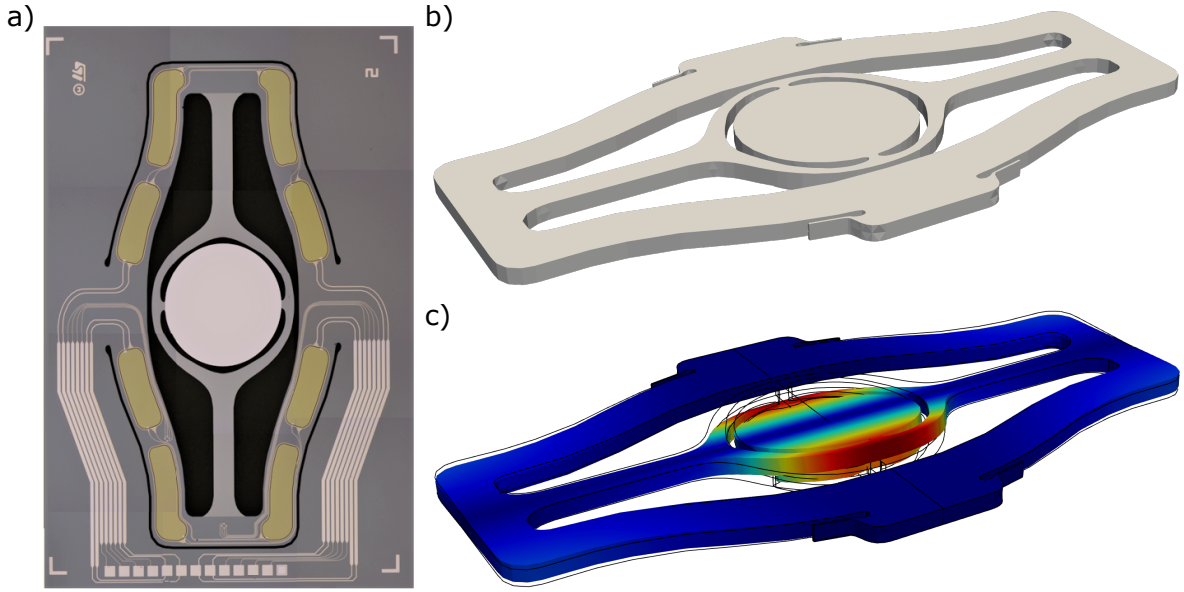

FIGURE 1 – (a) optical image of the MEMS micromirror. (b) geometry of the modeled device. (c) displacement field associated to the torsional mode, blue is the zero of the colour scale, red is the maximum of the colour scale.

2 Equations of motion and parametrisation method

The equation that governs the motion of geometrically nonlinear structures is the conservation of linear momentum with Saint Venant-Kirchhoff constitutive model. Its weak formulation in absence of body forces and surface traction is :

$$\int_\Omega \rho\, \ddot{\mathbf{u}} \cdot \mathbf{w}\, d\Omega + \int_\Omega \mathbf{e} : \mathcal{A} : \delta\mathbf{e}\, d\Omega = \mathbf{0}, \quad \forall \mathbf{w} \in \mathcal{C}(\mathbf{0}), \tag{1}$$

with ρ density, $\mathbf{u}$ displacement field, $\mathbf{w}$ test function defined over the space $\mathcal{C}(\mathbf{0})$ of functions that vanish on the boundary where Dirichlet boundary conditions on the displacement field are imposed. $\mathbf{e} = (\nabla\mathbf{u} + \nabla^T\mathbf{u} + \nabla^T\mathbf{u} \cdot \nabla\mathbf{u})/2$ Green-Lagrange Strain tensor, and $\delta\mathbf{e}$ first variation of the Green-Lagrange strain tensor. $\mathcal{A}$ is the fourth order elasticity tensor. All quantities are defined in material configuration Ω. We introduce a suitable finite element discretisation of Eq. (1) with nodal shape functions and we add Rayleigh damping :

$$\mathbf{M}\ddot{\mathbf{U}} + \mathbf{C}\dot{\mathbf{U}} + \mathbf{K}\mathbf{U} + \mathbf{G}(\mathbf{U},\mathbf{U}) + \mathbf{H}(\mathbf{U},\mathbf{U},\mathbf{U}) = \mathbf{0}, \tag{2}$$

with $\mathbf{M}$ mass matrix, $\mathbf{C}$ damping matrix, $\mathbf{K}$ stiffness matrix, and $\mathbf{U}$ displacement field. $\mathbf{U}$ is the nodal displacement vector. The damping matrix is taken as $\mathbf{C} = \alpha\mathbf{M} + \beta\mathbf{K}$ with α and β non negative scalars. $\mathbf{G}$ and $\mathbf{H}$ are quadratic and cubic nonlinearity tensors respectively. Eq. (2) has dimension N, which corresponds to the dimension of the finite dimensional spaces over which we restricted displacement and test fields in our problem. Eq. (2) is recasted in first order by introducing the velocity $\mathbf{V} = \dot{\mathbf{U}}$:

$$\mathbf{M}\dot{\mathbf{V}} + \mathbf{C}\mathbf{V} + \mathbf{K}\mathbf{U} + \mathbf{G}(\mathbf{U},\mathbf{U}) + \mathbf{H}(\mathbf{U},\mathbf{U},\mathbf{U}) = \mathbf{0}, \tag{3a}$$

$$\mathbf{M}\dot{\mathbf{U}} - \mathbf{M}\mathbf{V} = \mathbf{0}. \tag{3b}$$

Equation (3) is made by 2N equations. It has at least a fixed point for $(\mathbf{U},\mathbf{V}) = \mathbf{0}$. By linearising Eq. (3) at the origin the associated generalised eigenvalue problem provides the following left $\mathbf{X}_j$ and right $\mathbf{Y}_j$

eigenvectors and the eigenvalues λ_j :

$$\forall\, j = 1, ..., \mathrm{N},$$

$$\mathbf{X}_j = \frac{1}{\lambda_j - \bar{\lambda}_j} \begin{bmatrix} \phi_j \\ -\phi_j \bar{\lambda}_j \end{bmatrix}, \quad \mathbf{X}_{j+\mathrm{N}} = \bar{\mathbf{X}}_j = \frac{1}{\bar{\lambda}_j - \lambda_j} \begin{bmatrix} \phi_j \\ -\phi_j \lambda_j \end{bmatrix}, \tag{4a}$$

$$\mathbf{Y}_j = \begin{bmatrix} \phi_j \lambda_j \\ \phi_j \end{bmatrix}, \quad \mathbf{Y}_{j+\mathrm{N}} = \overline{\mathbf{Y}}_j = \begin{bmatrix} \phi_j \bar{\lambda}_j \\ \phi_j \end{bmatrix}, \tag{4b}$$

$$\lambda_j = -\xi_j \omega_j + i\omega_j \sqrt{1-\xi_j^2}, \quad \lambda_{j+\mathrm{N}} = \bar{\lambda}_j = -\xi_j \omega_j - i\omega_j \sqrt{1-\xi_j^2}, \tag{4c}$$

with ϕ_j eingenvectors associated to the linearised mechanical problem in Eq. (2), ω_j eigenfrequencies, and ξ_j modal damping coefficient. Dimensionality reduction is performed by parametrising the motion of the system along an invariant manifold tangent at the origin to the plane spanned by one of the linearised modes. This is achieved through the nonlinear polynomial coordinate change between nodal displacement and velocity and the nodal coordinates defined along the manifold $\mathbf{z}$:

$$\mathbf{U} = \boldsymbol{\Psi}(\mathbf{z}), \quad \mathbf{V} = \boldsymbol{\Upsilon}(\mathbf{z}). \tag{5}$$

The dynamics of the system onto the manifold as a function of the normal coordinates is formulated as :

$$\dot{\mathbf{z}} = \mathbf{f}(\mathbf{z}), \tag{6}$$

with $\mathbf{f}(\mathbf{z})$ polynomial function computed during the parametrisation procedure. Time derivatives of Eq. (5) are defined as :

$$\dot{\mathbf{U}} = \nabla_{\mathbf{z}} \boldsymbol{\Psi}(\mathbf{z}) \mathbf{f}(\mathbf{z}), \quad \dot{\mathbf{V}} = \nabla_{\mathbf{z}} \boldsymbol{\Upsilon}(\mathbf{z}) \mathbf{f}(\mathbf{z}). \tag{7}$$

Upon substitution of Eqs. (5) and (7) in Eq. (3) the invariance equation is obtained as :

$$\mathbf{M}\nabla_{\mathbf{z}} \boldsymbol{\Upsilon}(\mathbf{z}) \mathbf{f}(\mathbf{z}) + \mathbf{C}\boldsymbol{\Upsilon}(\mathbf{z}) + \mathbf{K}\boldsymbol{\Psi}(\mathbf{z}) + \mathbf{G}(\boldsymbol{\Psi}(\mathbf{z}), \boldsymbol{\Psi}(\mathbf{z})) + \mathbf{H}(\boldsymbol{\Psi}(\mathbf{z}), \boldsymbol{\Psi}(\mathbf{z}), \boldsymbol{\Psi}(\mathbf{z})) = \mathbf{0}, \tag{8a}$$

$$\mathbf{M}\nabla_{\mathbf{z}} \boldsymbol{\Psi}(\mathbf{z}) \mathbf{f}(\mathbf{z}) - \mathbf{M}\boldsymbol{\Psi}(\mathbf{z}) = \mathbf{0}, \tag{8b}$$

which represents an underdetermined set of algebraic equations since the dimension of the system is 2N, and the number of unknowns is provided by the 2N unknowns of the mappings and the 2n unknowns of the reduced dynamic coefficients, with n number of master modes. Efficient solution of the invariance equations is provided in [21], yielding the following equations that need to be solved up to a maximum order o :

$$\forall\, I \in \mathcal{H}^{(p)}, \forall\, p = 1, ..., o,$$

$$\mathbf{M}\boldsymbol{\Upsilon}_I^{(p)} \sigma_I + \sum_{s=1}^{2\mathrm{n}} \left(\mathbf{M}\phi_s \lambda_s f_{sI}^{(p)} \right) + \mathbf{M}\boldsymbol{\nu}_I^{(p)} + \mathbf{C}\boldsymbol{\Upsilon}_I^{(p)} + \mathbf{K}_I^{(p)} + \check{\mathbf{G}}_I^{(p)} + \check{\mathbf{H}}_I^{(p)} = \mathbf{0} \tag{9a}$$

$$\mathbf{M}\boldsymbol{\Psi}_I^{(p)} \sigma_I + \sum_{s=1}^{2\mathrm{n}} \left(\mathbf{M}\phi_s f_{sI}^{(p)} \right) + \mathbf{M}\boldsymbol{\mu}_I^{(p)} - \mathbf{M}\boldsymbol{\Upsilon}_I^{(p)} = \mathbf{0}, \tag{9b}$$

with I set of indexes associated to the normal coordinate monomials combination $\{i_1, ..., i_p\}$. The total number of combinations is collected in the set $\mathcal{H}^{(p)}$. All the remaining quantities are defined as :

$$\sigma_I = \lambda_{i_1} + \lambda_{i_2} + \ldots + \lambda_{i_p}, \tag{10a}$$

$$\boldsymbol{\mu}_I^{(p)} = \sum_{s=1}^{2\mathrm{n}} \sum_{k=2}^{p-1} \sum_{l=0}^{p-k} \boldsymbol{\Psi}_{i_1 \ldots i_l s i_{l+k+1} \ldots i_p}^{(p-k+1)} f_{s i_{l+1} \ldots i_{l+k}}^{(k)} \tag{10b}$$

$$\boldsymbol{\nu}_I^{(p)} = \sum_{s=1}^{2\mathrm{n}} \sum_{k=2}^{p-1} \sum_{l=0}^{p-k} \boldsymbol{\Upsilon}_{i_1 \ldots i_l s i_{l+k+1} \ldots i_p}^{(p-k+1)} f_{s i_{l+1} \ldots i_{l+k}}^{(k)} \tag{10c}$$

$$\check{\mathbf{G}}_I^{(p)} = \sum_{k=1}^{p-1} \mathbf{G}\left(\boldsymbol{\Psi}_{i_1 \ldots i_k}^{(k)}, \boldsymbol{\Psi}_{i_{k+1} \ldots i_p}^{(p-k)} \right), \tag{10d}$$

$$\check{\mathbf{H}}_I^{(p)} = \sum_{k=1}^{p-2} \sum_{l=1}^{p-k-1} \mathbf{H}\left(\boldsymbol{\Psi}_{i_1 \ldots i_k}^{(k)}, \boldsymbol{\Psi}_{i_{k+1} \ldots i_{k+1}}^{(l)}, \boldsymbol{\Psi}_{i_{k+1+1} \ldots i_p}^{(p-k-l)} \right). \tag{10e}$$

Solution of Eq. (9) provides both reduced dynamics law $\mathbf{f}(\mathbf{z})$ and mappings $\mathbf{\Psi}(\mathbf{z})$, $\mathbf{\Upsilon}(\mathbf{z})$. At order 1, Eq. (9) is satisfied by the linear mode and eigenvalues which are enforced on the structure of mappings and reduced dynamics. This ensures the identity tangency property to the linear eigenspace.

3 Scanning micromirror, high order nonlinearities

Scanning micromirrors represent key components in several Indutry 4.0 applications. In general, almost every high end application that requires accurate control of optical signals embeds a MEMS micromirror. Among the main industrial application we find Microsoft® Hololens™ and Intel® RealSense™ LiDAR camera.
Fast and accurate design of this class of devices is one of the main technological challenges of the semiconductor industry since the large configuration changes these devices experience during actuation lead to geometrical nonlinear effects. As a consequence, model order reduction techniques based on linear transformations often fail or require excessive computational effort to be used during the design stage of these components. In this section, we show how the presented method overcomes these difficulties.

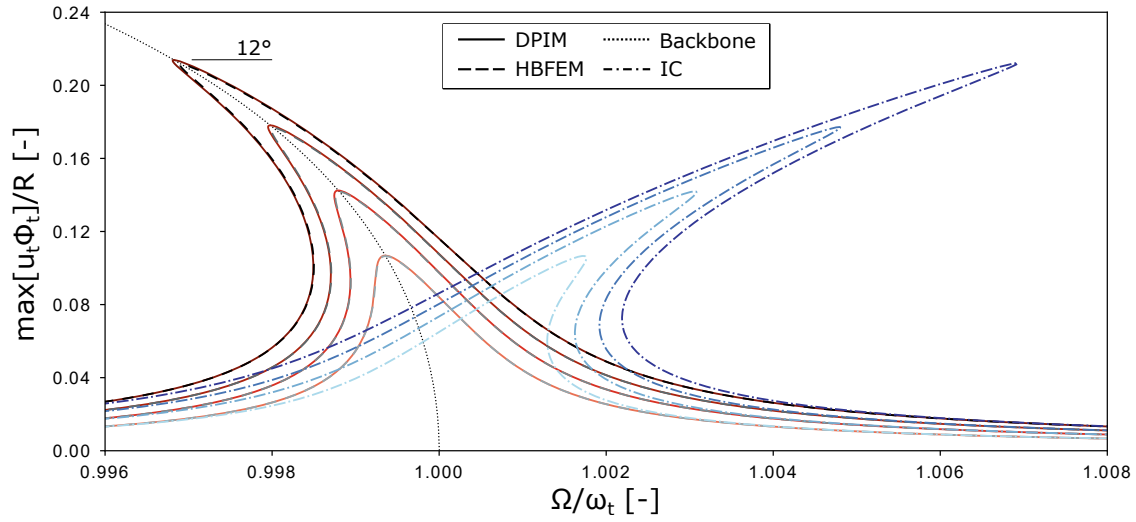

FIGURE 2 – Frequency response curves obtained for the scanning micromirror under investigation for forcing value κ equal to 1.5, 2.0, 2.5, and 3.0 μm/μs^2. The undamped-unforced response of the system (backbone) obtained from the reduced model is reported for reference. The maximum rotation angle experienced by the device is approximately equal to 12° as reported by the tag in the chart. Amplitudes are normalised by the radius R of the mirror reflective surface.

The device under examination is a MEMS micromirror developed by STMicroelectronics®. A picture of the device, its discretised geometry, and the torsional mode ϕ_t of the device are reported in Fig. 1. This system is made in monocrystalline silicon with the [110] orientation aligned with the axis of central torsional beams of the structure [22]. The real structure is actuated with patches of lead-zirconate titanate (PZT). In the present work, the structure is actuated with a body force proportional to the torsional mode of the structure. This ensures that exact accuracy at zero order of the method is obtained by simply projecting the force onto the torsional mode and by adding it to the reduced dynamics through proper coordinate change [19, 21], if parametrisation is performed with either graph style or real normal form style. Dissipation is introduced as Rayleigh damping with $\alpha = \omega_t/Q$ and $\beta = 0$, with ω_t resonance frequency of the torsional mode, and Q quality factor of the structure. ω_t is equal to 0.1839 rad/μs and Q is chosen equal to 1000. The resulting model is :

$$\mathbf{M}\ddot{\mathbf{U}} + \mathbf{C}\dot{\mathbf{U}} + \mathbf{K}\mathbf{U} + \mathbf{G}(\mathbf{U},\mathbf{U}) + \mathbf{H}(\mathbf{U},\mathbf{U},\mathbf{U}) = \kappa\mathbf{M}\phi_t cos(\Omega t), \tag{11}$$

with Ω forcing frequency, t time, and κ load multiplier. The structure geometry is discretised with 15-nodes quadratic wedge elements for a total of 9732 degrees of freedom. Dimensionality reduction is

performed through parametrisation of the system along the spectral submanifold tangent at the origin to the linear torsional mode. Parametrisation style is graph style and expansion order is varied up to order 9. Validation of the model is performed by solving the full order model with the Harmonic Balance Finite Element Method with arc-length continuation. To highlight the benefits of adopting the presented approach over similar state-of-the art techniques comparison with the predictions provided by the IC method are reported. Both reduced models obtained by the presented approach and by the IC method are solved by resorting to the continuation package BifurcationKit [23]. Validations are also performed with the continuation package ManLab [24].
Results are collected in Fig. 2, highlighting the perfect agreement of the proposed model with full order solutions. Several features must be highlighted. Frequency response curves are computed for κ values equal to 1.5, 2.0, 2.5, and 3 μm/μs^2. First of all, the reduced model (DPIM) perfectly captures the nonlinear dynamics response predicted by full order HBFEM simulations. This results is already observed in [21] and it is provided by the perfect ability of the method to include the velocity dependence of parametrised manifold. Furthermore, high order nonlinear terms introduced by the order 9 expansion ensure an excellent prediction of the structure nonlinearity even at high amplitudes. All these features are not reproduced by the IC method that fails at identifying the softening response of the structure, the latter also evidenced experimentally in [1]. This is consistent with the small transformations assumption of the IC method presented in [8], which succeeds in modeling highly nonlinear interactions in systems subjected to moderate rotations [25].

4 Arch Resonator, 1 :2 internal resonance

MEMS resonators are devices exploited for filtering, sensing and timing applications. While operation in the linear regime is well-established in industry, design of MEMS resonators that operate in the nonlinear regime is almost non-existent due to the lack of rapid predictive tools. In this setting, the proposed method is here applied to predict the response of an internally resonant arch resonator.

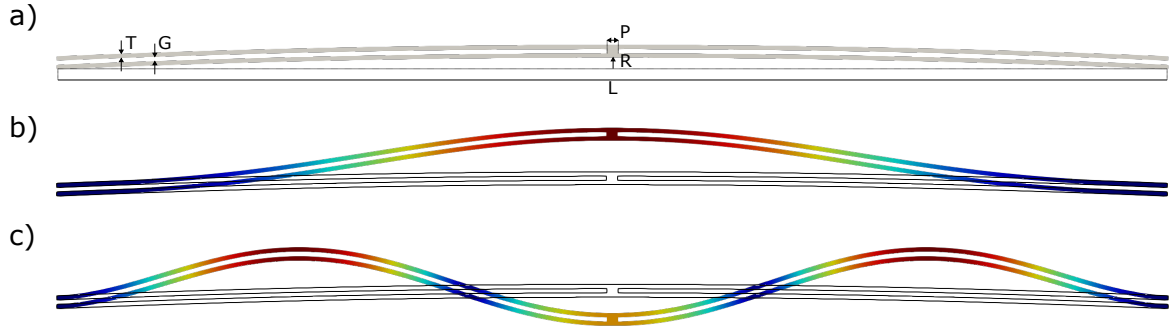

FIGURE 3 – (a) geometry of the internally resonant arch resonator. L = 649.5 μm, R = 6.675 μm, P = 6.5 μm, T = μm, and G = 2.5 μm. (b) drive mode displacement field. (c) coupled mode displacement field. blue is the zero of the colour scale, red is the maximum of the colour scale.

The geometry of the device is reported in Fig. 3a. It is made in polycrystalline silicon, which is modeled as isotropic with Young's modulus equal to 160 GPa and a Poisson's ratio equal to 0.22. The structure presents two coupled modes that satisfy a 1 :2 internal resonance condition. The first mode is reported in Fig. 3b and it has a resonance frequency of 0.8955 rad/μs. The coupled mode is reported in Fig. 3c and it has a resonance frequency of 0.1791 rad/μs. This internal resonance condition yields invariant breaking terms which in turn make the underlying invariant set four-dimensional. The two modes are labelled as mode 1 and mode 2. As for the mirror, a force proportional to mode 1 is applied :

$$\mathbf{M}\ddot{\mathbf{U}} + \mathbf{C}\dot{\mathbf{U}} + \mathbf{K}\mathbf{U} + \mathbf{G}(\mathbf{U},\mathbf{U}) + \mathbf{H}(\mathbf{U},\mathbf{U},\mathbf{U}) = \kappa\mathbf{M}\phi_1 cos(\Omega t), \tag{12}$$

where $\mathbf{C} = \frac{\omega_1}{Q}\mathbf{M}$, and Q is set equal to 1000 as for the micromirror. The system is discretised with 15-nodes quadratic wedge elements. Full order solutions are obtained with HBFEM simulations using

an order 9 expansion. The reduced model is obtained by parametrising the system along the invariant manifold tangent at the origin to mode 1 and mode 4 using an order 9 expansion with graph style.
Results obtained from the integration of the reduced model are reported in Fig. 4a for κ values equal to 0.01, 0.015, 0.02, and 0.025. Undamped responses of the reduced model are reported as well to highlight the positive and negative quadratic modes typical of the 1 :2 internal resonance [26]. The undamped response associated to the motion of mode 2 alone is reported as well in black dotted line. The comparison between full order simulations and reduced model are reported in Fig. 4b, where the amplitude associated to the internally resonant mode is reported. We highlight that since the applied force is collinear with mode 1, the resonance peaks associated to mode 2 are induced purely by the internal resonance condition. Overall, the agreement between full order simulations and reduced model is perfect even in presence of strong internal resonance conditions as those exhibited by this structure. Furthermore, as compared to the work presented in [19], adopting a high order graph style parametrisation provides improvement compared to low order approaches in real normal form style for systems that exhibit internal resonance.
Regarding the computational performance of the method, the original finite element model features 6471 degrees of freedom and its solution with the HBFEM required 2 days. An order 9 parametrisation with 2 master modes required 10 minutes to derive the model, and less than a minute to integrate the reduced model for all forcing levels combined.

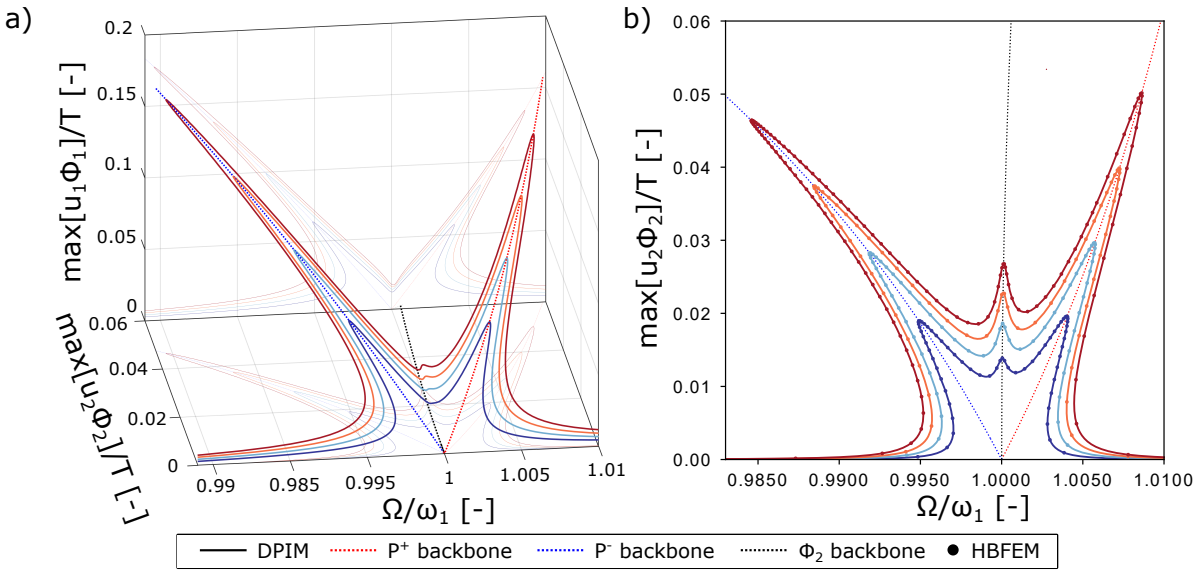

FIGURE 4 – (a) results obtained from the integration of the reduced model. (b) comparison between reduced model and HBFEM simulations. Both charts report the undamped response of the structure as well, highlighting the appearance of positive and negative quadratic modes also observed in the analytical developments by Gobat and coworkers [26]. The backbone associated to the second mode (ϕ_2 backbone) is reported at the frequency of the first mode. All undamped-unforced responses are obtained from the reduced model computed from the undamped system. κ values used during forced damped simulations are equal to 0.01, 0.015, 0.02, and 0.025 μm/μs^2, respectively.

5 Conclusion

In the present work we applied the high order direct parametrisation for invariant manifold method for the analysis of two classes of MEMS structures : a scanning micromirror and an arch resonator. As highlighted by the remarkable accuracy and unprecedented computational performance of the method, adopting nonlinear reduction method enables the accurate analysis of structures subjected to strong geometric nonlinearities within time-spans compatible with the design requirements of MEMS components.

6 Acknowledgments

The authors are grateful to STMicroelectronics® for the design of the MEMS micromirror and to Valentina Zega for the design of the MEMS arch resonator.

Références

[1] A. Opreni, N. Boni, R. Carminati, A. Frangi. *Analysis of the nonlinear response of piezo-micromirrors with the harmonic balance method*, Actuators, vol. 10(2), pp. 21, 2021

[2] M. Amabili, C. Touzé. *Reduced-order models for nonlinear vibrations of fluid-filled circular cylindrical shells : comparison of POD and asymptotic nonlinear normal modes methods*, Journal of Fluids and Structures, vol. 23(6), pp. 885-903, 2007

[3] G. Gobat, A. Opreni, S. Fresca, A. Manzoni, A. Frangi. *Reduced order modeling of nonlinear microstructures through Proper Orthogonal Decomposition*, arXiv, 2109.12184, 2021

[4] S. Shaw, C. Pierre. *Non-linear normal modes and invariant manifolds*, Journal of Sound and Vibration, vol. 150(1), pp. 170-173, 1991

[5] C. Touzé, A. Vizzaccaro, O. Thomas. *Model order reduction methods for geometrically nonlinear structures : a review of nonlinear techniques*, Nonlinear Dynamics, vol. 105, pp. 1141-1190, 2021

[6] S. Jain, P. Tiso, J.B. Rutzmoser, D.J. Rixen. *A quadratic manifold for model order reduction of nonlinear structural dynamics*, Computers & Structures, vol. 188, pp. 80-94, 2017

[7] J.J. Hollkamp, R.W. Gordon. *Reduced-order models for nonlinear response prediction : Implicit condensation and expansion*, Journal of Sound and Vibration, vol. 318(4-5), pp. 1139-1153, 2008

[8] A. Frangi, G. Gobat. *Reduced order modelling of the non-linear stiffness in MEMS resonators*, International Journal of Non-Linear Mechanics, vol. 116, pp. 211-218, 2019

[9] G. Haller, S. Ponsioen. *Exact model reduction by a slow–fast decomposition of nonlinear mechanical systems*, Nonlinear Dynamics, vol. 90, pp. 617-647, 2017

[10] A. Vizzaccaro, L. Salles, C. Touzé. *Comparison of nonlinear mappings for reduced-order modelling of vibrating structures : normal form theory and quadratic manifold method with modal derivatives*, Nonlinear Dynamics, vol. 103(4), pp. 3335-3370, 2021

[11] Y. Shen, A. Vizzaccaro, N. Kesmia, T. Yu, L. Salles, O. Thomas, C. Touzé. *Comparison of reduction methods for finite element geometrically nonlinear beam structures*, Vibration, vol. 4(1), pp. 175-204, 2021

[12] X. Cabré, E. Fontich, R. de la Llave. *The parameterization method for invariant manifolds. I. Manifolds associated to non-resonant subspaces*, Indiana Univ. Math. J., vol. 52(2), pp. 283-328, 2003

[13] X. Cabré, E. Fontich, R. de la Llave. *The parameterization method for invariant manifolds. II. Regularity with respect to parameters*, Indiana Univ. Math. J., vol. 52(2), pp. 329-360, 2003

[14] X. Cabré, E. Fontich, R. de la Llave. *The parameterization method for invariant manifolds. III. Overview and applications*, J. Differential Equations, vol. 218(2), pp. 444-515, 2005

[15] A. Haro, M. Canadell, J.L. Figueras, A. Luque, J.M. Mondelo. *The parameterization method for invariant manifolds*, Springer, 2016

[16] C. Touzé, M. Amabili. *Nonlinear normal modes for damped geometrically nonlinear systems : Application to reduced-order modelling of harmonically forced structures*, Journal of sound and Vibration, vol. 298(4-5), pp. 958-981, 2006

[17] A. Ponsioen, T. Pedergnana, G. Haller. *Automated computation of autonomous spectral submanifolds for nonlinear modal analysis*, Journal of sound and Vibration, vol. 420, pp. 269-295, 2018

[18] A. Vizzaccaro, Y. Shen, L. Salles, J. Blahoš, C.Touzé. *Direct computation of nonlinear mapping via normal form for reduced-order models of finite element nonlinear structures*, Computer Methods in Applied Mechanics and Engineering, vol. 384, pp. 113957, 2021

[19] A. Opreni, A. Vizzaccaro, A. Frangi, C. Touzé. *Model order reduction based on direct normal form : application to large finite element MEMS structures featuring internal resonance*, Nonlinear Dynamics, vol. 105, pp. 1237-1272, 2021

[20] S. Jain, G. Haller. *How to compute invariant manifolds and their reduced dynamics in high-dimensional finite element models*, Nonlinear Dynamics, in press, 2021

[21] A. Vizzaccaro, A. Opreni, L. Salles, A. Frangi, C. Touzé. *High order direct parametrisation of invariant manifolds for model order reduction of finite element structures : application to large amplitude vibrations and uncovering of a folding point*, arXiv, 2109.10031, 2021

[22] M.A. Hopcroft, .D. Nix, T.W. Kenny. *What is the Young's Modulus of Silicon ?*, Journal of microelectromechanical systems, vol. 19(2), pp. 229-238, 2010

[23] R. Veltz. *BifurcationKit.jl*, https ://hal.archives-ouvertes.fr/hal-02902346, 2020

[24] B. Cochelin, C. Vergez. *A high order purely frequency-based harmonic balance formulation for continuation of periodic solutions*, Journal of Sound and Vibration, vol. 324, pp. 243 - 262, 2009

[25] G. Gobat, V. Zega, P. Fedeli, L. Guerinoni, C. Touzé, A. Frangi. *Reduced order modelling and experimental validation of a MEMS gyroscope test-structure exhibiting 1 : 2 internal resonance*, Scientific Reports, vol. 11(1), pp. 1-8

[26] G. Gobat, L. Guillot, A. Frangi, B. Cochelin, C. Touzé. *Backbone curves, Neimark-Sacker boundaries and appearance of quasi-periodicity in nonlinear oscillators : application to 1 :2 internal resonance and frequency combs in MEMS*, Meccanica, vol. 56, pp. 1937-1969, 2021